

# Fabrication and Characterization of Beaded SiC Quantum Rings with Anomalous Red Spectral Shift

Shikuan Yang, Brian Kiraly, William Yi Wang, Shunli Shang, Bingqiang Cao, Haibo Zeng, Yanhui Zhao, Weizhou Li, Zi-Kui Liu, Weiping Cai,\* and Tony Jun Huang\*

Shape- and size-control of nanocrystals (NCs) is valuable in many aspects of modern science and technology.<sup>[1–9]</sup> Wet chemical methods are widely used in the synthesis of metal, metal oxide, and metal sulfide NCs with various shapes and dimensions in a controllable manner.<sup>[1–9]</sup> However, they are unsuitable for the synthesis of carbides and nitrides because of their high melting points (generally > 2000 °C) as well as a lack of appropriate precursors. Carbide and nitride NCs are of significant interest for biomedical applications and optical devices operated in extreme conditions, because they have high strength and unique optical properties while being chemically inert and biocompatible.<sup>[10–15]</sup> The properties of NCs are dependent on not only their constituent materials but also their geometries. Nanorings, for example, are important zero-dimensional nanostructures in many applications and they provide an excellent model to explore quantum-related properties.<sup>[16–19]</sup> Their fabrication, however, remains a significant challenge using existing fabrication methodologies.<sup>[20–22]</sup>

In this work, we show that beaded SiC nanorings (inner size: 3–10 nm; outer size: 9–20 nm) can be synthesized at room temperature by reactive laser ablation of a silicon wafer in an organic medium combined with a subsequent selective chemical etch. The prepared SiC nanorings exhibit apparent quantum confinement effects, emitting strong violet-blue photoluminescence under ultraviolet excitation. More importantly, an anomalous red spectral shift ascribed to collective effects between surface structures and quantum confinement is observed. This is the first experimental confirmation that surface reconstruction and termination dominates the optical properties of SiC NCs below a threshold diameter of 3 nm determined by theoretical calculations. The photoluminescence tunability, biocompatibility, non-toxicity, and chemical stability make SiC nanorings excellent candidates for applications in biomedicine (e.g., bio-imaging) and optical devices operating under extreme conditions (e.g., high-temperature, high-pressure, and/or highly corrosive environments). In principle, the fabrication technique presented here could also be extended into the fabrication of other carbide, nitride, and carbonitride nanostructures.

Our previous studies have shown that Si nanoparticles can be prepared with pulsed laser (Nd:YAG, 1064 nm) ablation of a Si target immersed in ethanol (about 8 mL).<sup>[23]</sup> Here we discover that beaded SiC nanorings can be generated when the laser ablation time is prolonged. In detail, when laser irradiation first strikes the silicon wafer, a silicon plasma is immediately formed at the surface of the wafer due to absorption of the high laser power (process I in **Figure 1**); the local temperature of this plasma could reach several thousand degrees Kelvin. At the same time, pyrolysis of the ethanol molecules located at the interface between the silicon plasma and the surrounding liquid produced free carbon species (e.g., atoms) (process II in **Figure 1**). The subsequent decrease in the temperature and pressure of the silicon plasma caused many silicon nuclei to be formed. Some of these silicon nuclei reacted with the surrounding carbon atoms, forming SiC nanoparticles (process III in **Figure 1**). Alternatively, the large amount of silicon nuclei favored aggregation energetics and gave rise to hollow or porous-like Si aggregates (process III in **Figure 1**). These pre-formed Si aggregates were heated to an ultrahigh temperature  $T_h$  (several thousand Kelvin) when they absorbed subsequent laser pulses. The high local temperature around the Si aggregates induced by laser irradiation again led to decomposition of the ethanol into carbon species (e.g., atoms or clusters) in the immediate vicinity of the hot Si aggregates. Finally, the highly active carbon species reacted with the hot silicon aggregates and gradually transformed into hollow or porous-like SiC aggregates (process IV in **Figure 1**). This chemical reaction (i.e., carbonization) is

Dr. S. Yang, Prof. W. Cai  
Key Lab of Materials Physics  
Anhui Key Lab of Nanomaterials  
and Nanotechnology  
Institute of Solid State Physics  
Chinese Academy of Sciences  
Hefei 230031, P. R. China  
E-mail: wpcail@issp.ac.cn

Dr. S. Yang, B. Kiraly, Y. Zhao, Prof. T. J. Huang  
Department of Engineering Science and Mechanics  
The Pennsylvania State University  
University Park, PA 16802-6812, USA  
E-mail: junhuang@psu.edu

W. Y. Wang, Dr. S. Shang, Prof. Z.-K. Liu  
Department of Materials Science and Engineering  
The Pennsylvania State University  
University Park, PA 16802, USA

Prof. B. Cao  
School of Materials Science and Engineering  
University of Jinan  
Jinan, 250022, P. R. China

Prof. H. Zeng  
Department of Material Science  
Nanjing University of Aeronautics and Astronautics (NUAA)  
Nanjing 210016, P. R. China

Prof. W. Li  
School of Materials Science and Engineering  
Guangxi University  
Nanning, 530004, P. R. China



DOI: 10.1002/adma.201202286

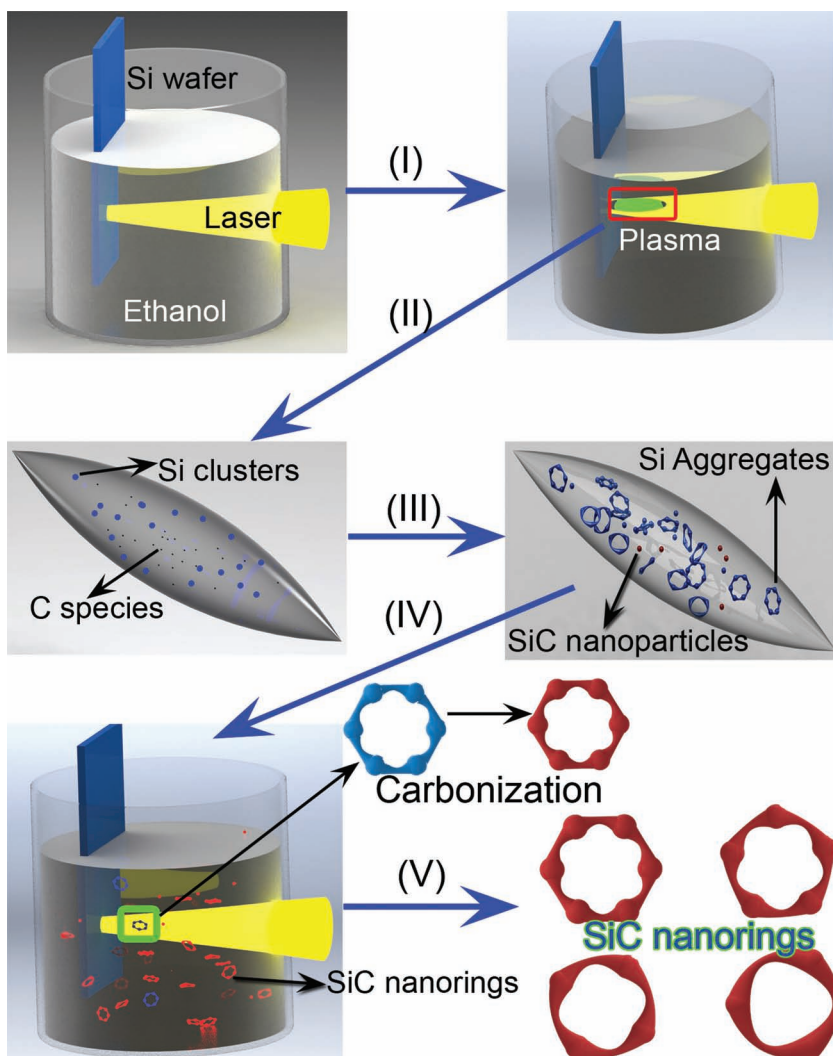


**Figure 1.** Schematic illustration of the formation process of SiC quantum rings. I, II) Laser-induced formation of Si plasma and carbon atoms/clusters. III) Formation of Si aggregates and SiC nanoparticles. IV) Transformation from Si aggregates to SiC nanorings by laser-induced carbonization. V) Selective etching of Si and centrifugation classification to generate pure SiC nanorings.

the reason for terming the method reactive laser ablation in liquid. As the Si–C reaction is restricted by small numbers of carbon atoms (only molecules near Si aggregates decompose) and ultra-short reaction times (short pulses lead to short durations of elevated temperature), a very small amount of Si can be transformed into SiC during a single laser shot exposure.<sup>[24]</sup> This condition necessitates many laser exposure cycles to transform the Si aggregates entirely into SiC. Hence, long-time laser irradiation is beneficial to the preparation of SiC nanorings. Finally, selective acid etching was used to remove the remaining Si and produce pure SiC nanorings/nanoparticles. Low-speed centrifugation is effective in separating SiC nanorings from SiC nanoparticles (process V in Figure 1).

Based on this mechanism, the laser energy density, which influences the amount of highly reactive carbon species present, and laser irradiation time, which affects the probability of Si nanoparticles secondary laser exposure, are both

crucial parameters for the preparation of SiC nanostructures. Transmission electron microscopy (TEM) images show that the as-prepared sample is seemingly composed of many nanoparticles (Figure S1a, Supporting Information). These nanoparticles are a mixture of Si and 3C–SiC, as verified by selected area electron diffraction (SAED) patterns (inset in Figure S1a) and X-ray photoelectron spectroscopy (XPS) results (Figures S2a and c, Supporting Information). Further analysis revealed that some of the as-prepared nanoparticles are hollow or porous-like aggregates (red arrows in Figure S1a, Supporting Information). The size distribution of the nanoparticles and the hollow or porous-like aggregates (measured as solid particles) are shown in Figures S1b and S1c, Supporting Information, which gives the mean size of 7.8 and 12.8 nm, respectively. A rough estimation indicates the hollow or porous-like aggregates comprise about 10% of the nanoparticles in the as-prepared sample.

An aqueous solution of HF (5 wt%) and H<sub>2</sub>O<sub>2</sub> (5 wt%) was used to remove the Si component from the as-prepared product. After the acid treatment (~5 h), the inner Si component has been completely removed and only SiC remains, as proved by the X-ray diffraction pattern (Figure S3, Supporting Information) and the Si 2p and C 1s XPS spectra (Figures S3b, d). Interestingly, a large amount of SiC nanorings emerge from this procedure, as shown in Figure 2a (see red arrow marks), with some nanorings not intact (green arrow marks in Figure 2a). There are also many ultra-fine SiC nanoparticles. The size distribution of the nanoparticles and nanorings (outer diameter of the “solid particle”) are exhibited in Figures 2b and 2c, showing mean diameters of 5.1 and 9.5 nm, respectively. Nanorings account

for approximately 15% of the nanoparticles in the pure SiC sample. Figures 2d–f present several typical SiC nanorings with different inner and outer diameters; the beaded structures are comprised of approximately 3 nm SiC quantum dots. The SiC nanorings can be separated from the SiC nanoparticles by a low-speed centrifugation classification method. This method allows pure narrow size distributions of SiC nanorings to be generated for further photoluminescence studies and applications, which is important in applications where size monodispersity is highly desired. By low-speed centrifugation classification (5000 rpm for 10 min), SiC nanorings were separated from the nanoparticles, and a large amount of SiC nanorings were obtained (Figure S5, Supporting Information). Figure 2g displays a cracked nanoring; the structure and morphology of the imperfect nanoring (Figure S6, Supporting Information) is significant because it verifies the formation mechanism of the SiC nanorings (Figure 1).

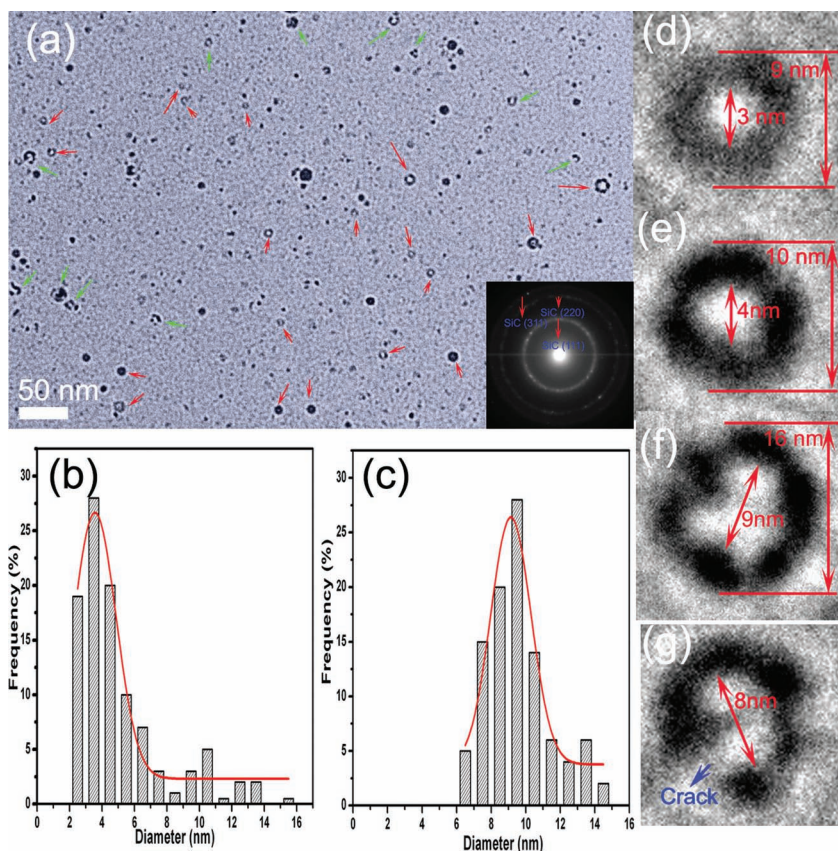


**Figure 2.** a) TEM image of 3C-SiC nanorings. Inset in (a), SAED of 3C-SiC. Size distribution of b) the nanoparticles and c) nanorings. d–f) typical 3C-SiC nanorings. g) a cracked nanoring.

The production rate of SiC nanorings is estimated to be  $20 \mu\text{g min}^{-1}$  by weighing the mass-loss of the Si target before and after the laser ablation process (detailed calculations can be found in the Supporting Information). There are several potential ways to increase the yield rate of SiC nanorings. By increasing the laser power and the laser frequency, the production rate of Si nanostructures can be accelerated, facilitating the mass production of SiC nanorings. Since an aromatic compound (i.e., toluene) is much easier to be decomposed into reactive carbon atoms by laser irradiation, the transformation efficiency from Si to SiC nanorings and thus the throughput of SiC nanorings is anticipated to be improved by adding a small amount of toluene into ethanol.

Laser ablation in liquid is usually deemed as a physical method to fabricate various semiconductor, metal, and metal oxide nanoparticle colloids.<sup>[25–30]</sup> Here, we first report that it can be extended to synthesize quantum-sized beaded SiC nanorings by introducing a carbonization reaction between the component from the Si target and carbon atoms and/or clusters induced by laser decomposition of the liquid molecules, which not only provides a method to prepare unique nanostructured carbide materials, but also deepens our understanding of the nanoparticle formation mechanism during the laser ablation in liquids. Taking advantage of the extremely high local temperature induced by laser ablation, this reactive laser ablation strategy might enable the fabrication of a wide variety of

nanostructures, such as  $\text{Si}_3\text{N}_4$ ,  $\text{C}_3\text{N}_4$ , TiC,  $\text{Fe}_3\text{C}$ , BN, and  $\text{W}_2\text{C}$ .<sup>[31]</sup> All of these carbide and nitride nanostructures have high strength (deducted from their corresponding bulk materials), strong chemical inertness, and resistance to heat, corrosion, and wear.

The SiC nanorings we synthesized demonstrate strong quantum confinement effects, so we denote them quantum rings. We found that SiC quantum rings show strong violet-blue emission with a peak centered at 430 nm under the excitation wavelength of 370 nm (see pink curve in Figure 3). As the photon energy of the emitted light is much larger than the bandgap of bulk 3C-SiC 2.25 eV (550 nm), such violet-blue emission is ascribed to quantum confinement effects, which is partially verified by UV-vis absorption spectra (Figure S7, Supporting Information). In addition, as the excitation wavelength is shifted from 350 to 460 nm, the emission peak moves from 418 to 510 nm (Figure 3). This blue spectral shift is a commonly observed phenomenon with a size distribution of quantum structures: as the excitation wavelength is decreased, smaller SiC NCs are excited, emitting shorter wavelengths because of their larger bandgaps (defined by quantum confinement).<sup>[32]</sup>

Surprisingly, when the excitation wavelength moves from 290 to 350 nm, the emission peak shifts from 432 to 418 nm (Figure 3): a red spectral shift. This red

shift contradicts theoretical predictions based on quantum confinement effects and has not been observed before in SiC NCs. In this case, an analogy to Si NCs might be helpful, as researchers have found that the optical bandgap of small sized Si nanoparticles is dramatically reduced when their surface is terminated with silicon–oxygen bonds instead of hydrogen.<sup>[33]</sup> Understanding that the surface area/volume ratio scales with  $1/r$ , we hypothesize that the surface atom configuration and the surface termination are overshadowing quantum confinement and determining the optical properties of the smaller SiC nanostructures. *Ab initio* calculations have made similar predictions for SiC NCs with a diameter between 1 and 3 nm,<sup>[34]</sup> however, the experimental evidence for  $< 3$  nm SiC NCs is still lacking because there are no appropriate techniques to prepare such small SiC NCs. There have already been reports that the surface structure (e.g., reconstruction or termination) of SiC NCs will influence their optical properties.<sup>[35]</sup> For example, SiC NCs with hydrogen and hydroxy bonding exhibit quite different optical properties, where a new peak at 510 nm emerges when the surface of SiC NCs is functionalized by  $\text{H}^+$  and  $\text{OH}^-$ .<sup>[35]</sup>

In order to explore the origin of the anomalous red spectral shift in our SiC quantum rings, we used a Gaussian multipeak fitting method to differentiate contributions from the surface structures and bandgap transitions within the SiC quantum rings to the photoluminescence emission spectrum. As shown in Figure S8, Supporting Information, there are two emission

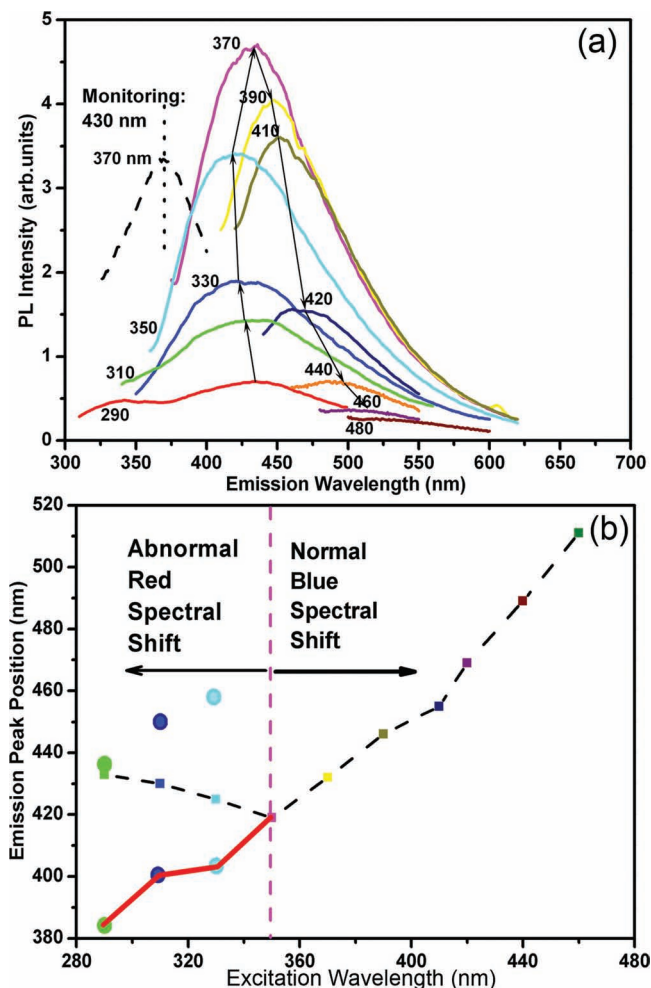


**Figure 3.** a) Photoluminescence (PL) spectra of 3C-SiC quantum rings under different excitation wavelengths and PL excitation spectrum monitoring at 430 nm (dashed line). b) Emission peak position as a function of excitation wavelength (black dashed line). The red line shows the peak position of the Gaussian fitted curve (in Figure S7) as a function of excitation wavelength.

peaks under the excitation wavelengths of 330 (Figure S8c) and 310 nm (Figure S8b), and three peaks at 290 nm excitation (Figure S8a). It is believed that the shorter-wavelength (404, 400, and 383 nm) emission peaks excited at 330, 310, and 290 nm can be attributed to bandgap transitions within SiC quantum rings. These three peaks (404, 400, and 383 nm) are in good accordance with the blue spectral shift induced by the quantum confinement effect (see red curve in Figure 3b).

To confirm that the longer-wavelength (434, 450, and 458 nm) emission peaks excited at 290, 310, and 330 nm have close relations to the surface structures of the SiC nanocrystals, we performed additional analysis, experiments, and theoretical calculations. Small sized SiC NCs can be deemed as formed by the core, exposed surfaces, and surface passivations. The core part generally contributes to the band-to-band recombinations, giving rise to the presence of the shorter-wavelength emission peaks (404, 400, and 383 nm) as aforementioned. Surface

passivations will have influence on the photoluminescence of SiC NCs. In order to determine the surface passivations of the SiC quantum rings, Fourier transform infrared (FTIR) characterization was conducted. From the FTIR result (Figure S9, Supporting Information) together with the Si 2p and C 1s XPS spectra (Figure S2), it is determined that the surfaces of SiC quantum rings are passivated by -OR (at Si sites) and -CH<sub>3</sub> (at C sites)—both -OR and -CH<sub>3</sub> are formed during laser decomposition of ethanol molecules. Based on the above-discussed SiC nanoring formation mechanism, the formation of these bonds on the surfaces of the SiC nanorings is not surprising. Laser ablation will decompose ethanol molecules into various reactive organic species and -OR. When SiC nanostructures are formed under the local high temperature induced by laser irradiation, these reactive organic species and -OH will bind to the surfaces of the SiC simultaneously. Due to the perfect surface passivations, surface defects are largely removed, resulting in the experimentally observed strong photoluminescence from the SiC quantum rings. However, these surface passivations (-CH<sub>3</sub> and -OR) are unlikely to lead to the anomalous red spectral shift according to previous studies.<sup>[35]</sup>

The surface structures of SiC NCs undergo serious energy favorable reconstructions as verified by theoretical calculations and experimental observations.<sup>[36]</sup> Different crystal planes have different atom reconfigurations and surface reconstructions. It is difficult to determine the exact exposed crystal planes of the SiC nanorings due to the irregular shapes of the nanorings and extremely non-equilibrium formation conditions. We took the (001) plane as an example and performed theoretical calculations based on first principles (details can be found in the Supporting Information). Our results (Figures S10, S11, Supporting Information) indicate that surface structures will introduce energy states within the bandgap. Interestingly, the results further reveal that carbon atoms on the surfaces contribute more significantly to the formation of these energy states compared with Si atoms (Figures S10, S11), indicating the importance of surface compositions to the electronic structures. Different crystal planes have different contributions to the band structure change of SiC NCs, unveiling the significance of atom configuration in changing the electronic structures of SiC NCs.<sup>[34]</sup> Therefore, surface structures of the SiC NCs including the surface composition (i.e., Si or C) and surface atom configuration (e.g., surface reconstructions and different exposed crystal planes) lead to the formation of energy states within bandgaps. The photon-excited excitons have two pathways to recombination (Figure S12, Supporting Information), i.e., band-to-band recombination (Process I in Figure S12) and recombination at the energy states induced by surface structures (Process II in Figure S12), resulting in the two emission peaks in Figure S7. The strain force within the SiC nanoring structure might also have an impact on the optical properties by influencing the band structure and/or affecting recombination pathways of excitons. In summary, surface composition and atom configuration connected with exposed crystal planes and surface reconstructions are important factors to the anomalous red spectral shift of SiC nanorings we observed.

Recently, red spectral shifts from Si nanocrystals were observed; they were ascribed to radiative recombination of non-equilibrium excitons.<sup>[37]</sup> This mechanism might also contribute

to the red spectral shift from our SiC quantum rings because of optical similarities between Si and SiC (e.g., intrinsic indirect bandgap). Photoluminescence peaks attributed to radiative defect centers can also affect the emission spectrum of Si NCs,<sup>[38]</sup> similar to the case in SiC quantum rings. However, the defect peak is usually well-separated from the bandgap peak in Si NCs, and further studies are needed to determine whether the mechanism we hypothesized above might contribute to the anomalous red spectral shift in Si NCs. Future investigations will measure the photoluminescence dynamics, the temperature dependence of the photoluminescence, and time-resolved photoluminescence to help classify the exact origin of the abnormal red spectral shift from SiC quantum rings.

The red spectral shift we observed from SiC quantum rings demonstrates that quantum confinement effects become invalid for calculating the optical bandgaps of SiC nanostructures when the size is very small. Below a threshold diameter ( $D_t$ ), the surface structure plays a significant role in determining the optical properties of the nanostructures. From Figure 3, we know that this transition occurs at approximately 350 nm excitation wavelength, and at this excitation wavelength, the SiC emission is located at about 420 nm (Figure 3). The emission energy can be defined as a function of particle size (Figure S12) according to quantum confinements using an effective mass approximation (Equation 1),<sup>[39]</sup>

$$E^* = E_g + \frac{h^2}{8\mu r^2} - 1.8e^2/4\pi\epsilon_0\epsilon r \quad (1)$$

where  $\mu = m_e m_h / (m_e + m_h)$  is the reduced mass of the exciton,  $m_e = 0.394m_0$ ,  $m_h = 0.387m_0$ , and  $m_0$  is the free electron mass.  $E_g$  is the band gap of bulk cubic SiC (2.25 eV),  $\epsilon$  is the high-frequency dielectric constant of SiC ( $\sim 10$ ), and  $r$  is the radius of the SiC NCs. Using this approximation, the threshold diameter ( $D_t$ ) for SiC NCs is calculated to be 3 nm. When the diameter of SiC NCs is below 3 nm, the contributions of surface structure (e.g., surface composition, surface reconstruction, and exposed crystal planes) to the photoluminescence emission cannot be neglected and they will play an important role together with quantum confinement effects. This is the first experimental work to point out the importance of surface structures of small sized (<3 nm) SiC nanostructures, which might cause contradictory spectral shift (i.e., red spectral shift) with the predictions based on quantum confinement effects.

The third peak (340 nm) under the excitation wavelength of 290 nm can be related to the interior structure evolution of the ultrafine SiC nanocrystals. The weak 383 nm peak, related to quantum confinement effects, indicates that the particle size can be roughly estimated at 2.6 nm (Figure S12). This peak indicates that as the size of the SiC NCs is further decreased below  $D_t$ , bandgap transitions are sharply weakened and surface structure contributions become overwhelmingly dominant. Under this condition, new ultraviolet emission peaks (e.g., 340 nm peak) will emerge with quite different origins (e.g., direct-bandgap like emissions)<sup>[40]</sup> due to the energetically favorable structural reconstruction of SiC NCs.

The photoluminescence from the SiC quantum rings we fabricated is very stable—it is still very intense even after several months of preservation. These non-toxic and biocompatible 3C–SiC quantum rings with strong and steady violet-blue emission will be invaluable in applications such as cell imaging,

bio-labeling, drug carrier, and optical devices operating under extreme conditions (e.g., high-temperature, high-frequency, high-pressure, and/or highly corrosive).

In summary, SiC quantum rings have been synthesized using reactive laser ablation of a Si target in ethanol combined with subsequent selective chemical etching. The SiC quantum rings show strong and steady violet-blue emissions, which exhibit a prominent excitation wavelength dependence (blue spectral shift) caused by quantum confinement effects when the excitation wavelength is larger than 350 nm. Interestingly, the SiC quantum rings also show an abnormal red spectral shift when the excitation wavelength is smaller than 350 nm, which is likely caused by surface structures (e.g., surface composition, surface reconstruction, and exposed crystal planes) in the smallest SiC NCs. Smaller than a threshold size (about 3 nm), surface structures must be considered when designing the optical properties of SiC NCs. The SiC quantum rings presented here have many desirable properties such as chemical inertness, high strength, fascinating optical properties, and interesting morphology (beaded rings). Importantly, the reactive laser ablation method might be conveniently extended to design other carbide and nitride nanostructures, compensating for the shortcomings of traditional chemical methods in preparing these nanomaterials.

## Supporting Information

Supporting Information is available from the Wiley Online Library or from the author.

## Acknowledgements

The authors gratefully acknowledge the financial support from National Institutes of Health (Director's New Innovator Award, 1DP2OD007209-01), National Science Foundation, Air Force Office of Scientific Research (AFOSR), the Penn State Center for Nanoscale Science (MRSEC), and National Science Foundation of China (Grant No. 50831005). Components of this work were conducted at the Penn State node of the NSF-funded National Nanotechnology Infrastructure Network.

Received: June 6, 2012  
Published online: August 22, 2012

- [1] R. Contreras-Caceres, J. Pacifico, I. Pastoriza-Santos, J. Perez-Juste, A. Fernandez-Barbero, L. M. Liz-Marzan, *Adv. Funct. Mater.* **2009**, *19*, 3070.
- [2] E. C. Cho, P. H. C. Camargo, Y. N. Xia, *Adv. Mater.* **2010**, *22*, 744.
- [3] M. Grzelczak, B. Rodriguez-Gonzalez, J. Perez-Juste, L. M. Liz-Marzan, *Adv. Mater.* **2007**, *19*, 2262.
- [4] Y. Sun, Y. Xia, *Science* **2002**, *298*, 2176.
- [5] Y. Xia, Y. Xiong, B. Lim, S. E. Skrabalak, *Angew. Chem. Int. Ed.* **2009**, *48*, 60.
- [6] S. E. Skrabalak, J. Chen, L. Au, X. Lu, X. Li, Y. N. Xia, *Adv. Mater.* **2007**, *19*, 3177.
- [7] G. Dukovic, M. G. Merkle, J. H. Nelson, S. M. Hughes, A. P. Alivisatos, *Adv. Mater.* **2008**, *20*, 4306.
- [8] M. H. Huang, P.-H. Lin, *Adv. Funct. Mater.* **2012**, *22*, 14.
- [9] X. S. Fang, T. Y. Zhai, U. K. Gautam, L. Li, L. M. Wu, Y. Bando, D. Golberg, *Prog. Mater. Sci.* **2011**, *56*, 175.

- [10] V. G. Pol, S. V. Pol, A. Gedanken, *Adv. Mater.* **2011**, *23*, 1179.
- [11] C. Giordano, A. Kraupner, S. C. Wimbush, M. Antonietti, *Small* **2010**, *6*, 1859.
- [12] J. Y. Fan, H. X. Li, J. Liang, L. K. Y. So, Y. W. Lam, P. K. Chu, *Small* **2008**, *4*, 1058.
- [13] C. Giordano, M. Antonietti, *Nano Today* **2011**, *6*, 366.
- [14] C. Giordano, C. Erpen, W. T. Yao, M. Antonietti, *Nano Lett.* **2008**, *8*, 4659.
- [15] J. Y. Fan, X. L. Wu, P. K. Chu, *Prog. Mater. Sci.* **2006**, *51*, 983.
- [16] K. A. Matveev, A. I. Larkin, L. I. Glazman, *Phys. Rev. Lett.* **2002**, *89*, 096802.
- [17] A. Lorke, R. J. Luyken, A. O. Govorov, J. P. Kotthaus, *Phys. Rev. Lett.* **2000**, *84*, 2223.
- [18] M. Grochol, R. Zimmermann, *Phys. Rev. B* **2007**, *76*, 195326.
- [19] K. Brunner, G. Abstreiter, G. Bohm, G. Trankle, G. Wilmann, *Phys. Rev. Lett.* **1994**, *73*, 1138.
- [20] L. Landin, M. S. Miller, M.-E. Pistol, C. E. Pryor, L. Samuelson, *Science* **1998**, *280*, 262.
- [21] L. Wang, F. Montagne, P. Hoffmann, R. Pugin, *Chem. Commun.* **2009**, 3798.
- [22] K. L. Hobbs, P. R. Larson, G. D. Lian, J. C. Keay, M. B. Johnson, *Nano Lett.* **2004**, *4*, 167.
- [23] S. K. Yang, W. P. Cai, H. W. Zhang, X. X. Xu, H. B. Zeng, *J. Phys. Chem. C* **2009**, *113*, 19091.
- [24] S. K. Yang, W. P. Cai, H. B. Zeng, X. X. Xu, *J. Mater. Chem.* **2009**, *19*, 7119.
- [25] a) K. Y. Niu, J. Yang, S. A. Kulinich, J. Sun, H. Li, X. W. Du, *J. Am. Chem. Soc.* **2011**, *1321*, 9814; b) K. Y. Niu, H. M. Zheng, Z. Q. Li, J. Yang, J. Sun, X. W. Du, *Angew. Chem. Int. Ed.* **2011**, *50*, 4099; c) K. Y. Niu, J. Yang, S. A. Kulinich, J. Sun, X. W. Du, *Langmuir* **2011**, *26*, 16652.
- [26] a) S. K. Yang, W. P. Cai, L. C. Kong, Y. Lei, *Adv. Funct. Mater.* **2010**, *20*, 2527; b) S. K. Yang, W. P. Cai, H. B. Zeng, Z. G. Li, *J. Appl. Phys.* **2008**, *104*, 023516; c) S. K. Yang, W. Z. Li, B. Q. Cao, H. B. Zeng, W. P. Cai, *J. Phys. Chem. C* **2011**, *115*, 21056; d) S. K. Yang, H. B. Zeng, H. P. Zhao, H. W. Zhang, W. P. Cai, *J. Mater. Chem.* **2011**, *21*, 4432; e) S. K. Yang, W. P. Cai, G. Q. Liu, H. B. Zeng, *J. Phys. Chem. C* **2009**, *113*, 7692; f) H. B. Zeng, G. T. Duan, Y. Li, S. K. Yang, X. X. Xu, W. P. Cai, *Adv. Funct. Mater.* **2010**, *20*, 561.
- [27] a) G. W. Yang, *Prog. Mater. Sci.* **2007**, *52*, 648; b) P. Liu, Y. Liang, X. Z. Lin, C. X. Wang, G. W. Yang, *ACS Nano* **2011**, *5*, 4748; c) P. Liu, Y. L. Cao, C. X. Wang, X. Y. Chen, G. W. Yang, *Nano Lett.* **2008**, *8*, 2570.
- [28] a) H. Usui, Y. Shimizu, T. Sadaki, N. Koshizaki, *J. Phys. Chem. B* **2005**, *109*, 120; b) H. Usui, T. Sasaki, N. Koshizaki, *J. Phys. Chem. B* **2006**, *110*, 12890; c) H. Usui, T. Sadaki, N. Koshizaki, *Appl. Phys. Lett.* **2005**, *87*, 063105.
- [29] a) J. Jakobi, S. Petersen, A. Menendez-Manjon, P. Wagener, S. Barcikowski, *Langmuir* **2010**, *26*, 6892; b) S. Barcikowski, A. Menendez-Manjon, B. Chichkov, M. Brikas, G. Raciukaitis, *Appl. Phys. Lett.* **2007**, *91*, 083113; c) C. L. Sajti, R. Sattari, B. N. Chichkov, S. Barcikowski, *J. Phys. Chem. C* **2010**, *114*, 2421; d) S. Barcikowski, A. Menendez-Manjon, B. Chichkov, M. Brikas, G. Raciukaitis, *Appl. Phys. Lett.* **2007**, *91*, 083113; e) C. L. Sajti, R. Sattari, B. N. Chichkov, S. Barcikowski, *J. Phys. Chem. C* **2010**, *114*, 2421.
- [30] a) F. Mafune, J. Kohno, Y. Takeda, T. Kondow, H. Sawabe, *J. Phys. Chem. B* **2000**, *104*, 9111; b) F. Mafune, J. Y. Kohno, Y. Takeda, T. Kondow, *J. Phys. Chem. B* **2003**, *107*, 4218; c) Z. J. Yan, R. Q. Bao, R. N. Wright, D. B. Chrisey, *Appl. Phys. Lett.* **2010**, *97*, 124106; d) Z. J. Yan, R. G. Bao, Y. Huang, D. B. Chrisey, *J. Phys. Chem. C* **2010**, *114*, 11370.
- [31] Reactive laser ablation has been successfully extended in the generation of  $W_2C$  NCs. The catalytic performance of the synthesized  $W_2C$  NCs is under study.
- [32] a) X. L. Wu, J. Y. Fan, T. Qiu, X. Yang, G. G. Siu, P. K. Chu, *Phys. Rev. Lett.* **2005**, *94*, 026102; b) J. Y. Fan, H. X. Li, W. N. Cui, D. J. Dai, P. K. Chu, *Appl. Phys. Lett.* **2010**, *97*, 191911; c) J. Y. Fan, H. X. Li, J. Liang, L. K. Y. So, Y. W. Lam, P. K. Chu, *Small* **2008**, *4*, 1058; d) J. Y. Fan, H. X. Li, Q. J. Wang, D. J. Dai, P. K. Chu, *Appl. Phys. Lett.* **2011**, *98*, 081913; e) J. Y. Fan, X. L. Wu, H. X. Li, H. W. Liu, G. G. Siu, P. K. Chu, *Appl. Phys. Lett.* **2006**, *88*, 041909; f) J. Y. Fan, X. L. Wu, R. Kong, T. Qiu, G. S. Huang, *Appl. Phys. Lett.* **2005**, *86*, 171903.
- [33] M. V. Wolkin, J. Jorne, P. M. Fauchet, G. Allan, C. Delerue, *Phys. Rev. Lett.* **1999**, *82*, 197.
- [34] a) A. Kassiba, M. Makowska-Janusik, J. Boucle, *Phys. Rev. B* **2002**, *66*, 155317; b) F. A. Reboredo, L. Pizzagalli, G. Galli, *Nano Lett.* **2004**, *4*, 801.
- [35] a) X. L. Wu, S. J. Xiong, J. Zhu, J. Wang, J. C. Shen, P. K. Chu, *Nano Lett.* **2009**, *9*, 4053; b) J. Wang, S. J. Xiong, X. L. Wu, T. H. Li, P. K. Chu, *Nano Lett.* **2010**, *10*, 1466.
- [36] a) P. Soukiassian, F. Semond, L. Douillard, A. Mayne, G. Dujardin, L. Pizzagalli, C. Joachim, *Phys. Rev. Lett.* **1997**, *78*, 907; b) F. Semond, P. Soukiassian, A. Mayne, G. Dujardin, L. Douillard, C. Jaussaud, *Phys. Rev. Lett.* **1996**, *77*, 2013; c) C. W. Hu, A. Kasuya, S. Suto, A. Wawro, Y. Nishina, *Appl. Phys. Lett.* **1996**, *68*, 253; d) P. G. Soukiassian, H. B. Enriquez, *J. Phys.: Condens. Matter* **2004**, *16*, S1611.
- [37] W. D. A. M. De Boer, D. Timmerman, K. Dohnalova, I. N. Yassievich, H. Zhang, W. J. Buma, T. Gregorkiewicz, *Nat. Nanotechnol.* **2010**, *5*, 878.
- [38] S. Godefroo, M. Hayne, M. Jivanescu, A. Stesmans, M. Zacharias, O. I. Lebedev, G. Van Tendeloo, V. V. Moshchalkov, *Nat. Nanotechnol.* **2008**, *3*, 174.
- [39] a) L. Brus, *J. Phys. Chem.* **1986**, *90*, 2555; b) X. L. Wu, G. G. Siu, C. L. Fu, H. C. Ong, *Appl. Phys. Lett.* **2001**, *78*, 2285.
- [40] The 340 nm PL peak under the excitation wavelength of 290 nm might originate from the direct transitions, since when the size of SiC nanostructures are very small (i.e., 2.6 nm), they may turn to direct bandgap. Calculations through density functional theory have predicted that SiC nanotubes have direct bandgaps when they are fully saturated (see R. L. Zhou, R. Z. Zuo, L. Wang, B. H. Zhang, B. C. Pan, *J. Appl. Phys.* **2011**, *109*, 084318). Such kind of direct-bandgap transition of Si NCs has been theoretically predicted and experimentally observed. The detailed origin of the 340 nm peak will be studied further.